Defective Choroidal Blood Flow Baroregulation and Retinal Dysfunction and Pathology Following Sympathetic Denervation of Choroid

Chunyan Li,[1] Malinda E. C. Fitzgerald,[1–3] Nobel Del Mar,[1] Corey Haughey,[1,3] and Anton Reiner[1,2]

[1]Department of Anatomy and Neurobiology, University of Tennessee Health Science Center, Memphis, Tennessee, United States
[2]Department of Ophthalmology, University of Tennessee, Memphis, Tennessee, United States
[3]Department of Biology, Christian Brothers University, Memphis, Tennessee, United States

PURPOSE. We sought to determine if sympathetic denervation of choroid impairs choroidal blood flow (ChBF) regulation and harms retina.

METHODS. Rats received bilateral superior cervical ganglionectomy (SCGx), which depleted choroid of sympathetic but not parasympathetic innervation. The flash-evoked scotopic ERG and visual acuity were measured 2 to 3 months after SCGx, and vasoconstrictive ChBF baroregulation during high systemic arterial blood pressure (ABP) induced by LNAME was assessed by laser Doppler flowmetry (LDF). Eyes were harvested for histologic evaluation.

RESULTS. ChBF increased in parallel with ABP in SCGx rats over an ABP range of 90% to 140% of baseline ABP, while in sham rats ChBF remained stable and uncorrelated with ABP. ERG a- and b-wave latencies and amplitudes, and visual acuity were significantly reduced after SCGx. In SCGx retina, Müller cell GFAP immunolabeling was upregulated 2.5-fold, and Iba1+ microglia were increased 3-fold. Dopaminergic amacrine cell fibers in inner plexiform layer were reduced in SCGx rats, and photoreceptors were slightly depleted. Functional deficits and pathology were correlated with impairments in sympathetic regulation of ChBF.

CONCLUSIONS. These studies indicate that sympathetic denervation of choroid impairs ChBF baroregulation during elevated ABP, leading to choroidal overperfusion. This defect in ChBF regulation is associated with impaired retinal function and retinal pathology. As sympathetic ChBF baroregulatory defects have been observed in young individuals with complement factor H (CFH) polymorphisms associated with risk for AMD, our results suggest these defects may harm retina, perhaps contributing to AMD pathogenesis.

Keywords: choroidal blood flow (ChBF), superior cervical ganglion (SCG), retinal degeneration, autonomic, sympathetic

The choroid is adaptively regulated by parasympathetic vasodilatory and sympathetic vasoconstrictory nerve fibers.[1–4] The pterygopalatine ganglion (PPG) mediates parasympathetic control, uses nitric oxide (NO) and vasoactive intestinal polypeptide (VIP) as vasodilators, and appears to play a role in adaptive choroidal vasodilation that stabilizes ChBF during bouts of reduced systemic blood pressure (BP).[5] The superior cervical ganglion (SCG) mediates choroidal vasoconstriction, and uses noradrenaline and NPY as vasoconstrictors.[4] Sympathetic innervation of choroid becomes activated with high BP, serving to vasoconstrict choroid to prevent overperfusion.[6–12] Diminished parasympathetic innervation of human choroid is observed with aging,[13] which may cause diminished ChBF and retinal ischemia that contributes to age-related declines. More recently, Told et al.[14] reported impaired stabilization of ChBF during high systemic BP in young individuals with a CFH risk haplotype for AMD, thus raising the possibility that impaired sympathetic control of ChBF might also harm the retina, and in some cases set the stage for AMD. In the present study, we show that sympathetic denervation of choroid via SCGx impairs the ability of ChBF to remain stable during high BP, and leads to retinal histopathologies and functional deficits within 1 to 3 months. Thus, impairment in the ability of ChBF to baroregulate in response to high systemic BP has rapid adverse effects on the retina, suggesting that sustained deficits of this type could be harmful in humans.

METHODS

Animals and Experiment Design

Adult male Sprague-Dawley rats (330–470 g; Harlan, Indianapolis, IN) were randomly assigned to either sham surgery or SCGx. For seven sham and seven SCGx rats, ERG and visual acuity were assessed for both eyes before surgery, and again 2 to 3 months' postsurgery. For these rats, ChBF was subsequently measured for both eyes by laser Doppler flowmetry (LDF), while monitoring systemic arterial BP (ABP). The rats were sacrificed and perfused with fixative after LDF, and eyes harvested for histological analysis. We killed 11 additional sham and 9 additional SCGx rats without prior functional assessments for histologic analysis alone 1 to 2 months after surgery. The shorter time point was used only for Müller cell analysis because GFAP upregulation in Müller cells is a sensitive early

marker of retinal injury. All experiments were in compliance with the ARVO Statement for the Use of Animals in Ophthalmic and Vision Research, and with National Institutes of Health and institutional guidelines.

SCGx Surgery

Rats were anesthetized with intraperitoneal ketamine/xylazine (87/13 mg/kg). The ventral neck was shaved, skin disinfected with povidone-iodine followed by 70% alcohol, and a 2.5 to 3 cm incision made at its midline. The common carotid artery was dissected cranially to its bifurcation into the external and internal carotid arteries, and the bifurcation moved laterally to expose the SCG, which was removed bilaterally. Our surgical procedure has been described by Savastano et al.,[15] and in a prior study of ours.[16] SCGx efficacy was confirmed by ptosis, and immunohistochemical evaluation of sympathetic innervation of choroid. Although the SCG projection to choroid is largely unilateral,[17] bilateral SCGx ensured all sympathetic innervation was eliminated. For two rats, we cut the ascending sympathetic trunk to the SCG bilaterally, to evaluate preganglionic deafferentation of SCG. Rats with superior cervical ganglion removal and superior cervical ganglion deafferentation were used in analysis of ABP, ChBF, ERG, visual acuity, retinal VMAT2, and ONL counts. The results were similar with superior cervical ganglion removal as with superior cervical ganglion deafferentation, and as a result both are referred to here as SCGx, and the data combined. Only rats with complete SCG removal were used in the GFAP and IBA1 analysis.

Electroretinography

ERGs were recorded using an ganzfeld ERG system (Ganzfeld; Diagnosys LLC, Lowell, MA, USA). After overnight dark adaptation, rats were anesthetized by intraperitoneal ketamine/xylazine (87/13 mg/kg), and each eye dilated with 1% cyclopentolate hydrochloride (Akorn, Lake Forest, IL, USA). Tail and forehead were sanitized with a sterile ethanol swab prior to insertion of a subcutaneous ground and reference electrode, respectively. A drop of methylcellulose gel (2% Methocel; OmniVision, Neuhausen, Switzerland) was applied to the cornea of each eye, and either silver pad electrodes or gold ring electrodes (3 mm diameter Goldring; Roland Consult, Brandenburg, Germany) were positioned on the corneal surface, with pre-post measurements made with the same electrode type. A binocular flash stimulator (Color-Dome; Diagnosys LLC) was centered over the rat, and seven light intensities presented multiple times: 0.0001, 0.001, 0.01, 0.1, 1, 10, 758 scot cd/m^2. The mean a- and b-wave amplitudes and latencies were determined for each with a custom routine (Igor Pro version 6.37), and exported to spreadsheet software (Excel; Microsoft, Redmond, WA, USA). We performed 1-way ANOVA with posthoc comparisons using statistical software (IBM SPSS version 22) to compare SCGx to sham ERG in terms of change from presurgery values, with eyes pooled.

Visual Acuity

Visual acuity was assessed using a virtual cylinder optokinetic system (OptoMotry, CerebralMechanics, Alberta, Canada), as described previously.[18,19] The experimenter was blinded to the stimulus and the eye tested during the scoring of stimulus responses during each trial. Stimuli that varied in spatial frequency (at 100% contrast) were presented trial-by-trial by a staircase method until a threshold was determined for each eye.

Choroidal Blood Flow and Baroregulation

Following completion of visual testing, rats were anesthetized with ketamine/xylazine for ChBF assessment, as described previously.[20-24] The right femoral artery was cannulated for monitoring ABP via a pressure transducer (TXD-310, Micro-Med Inc.; Louisville, KY, USA) and a blood pressure analyzer (Digi-Med, BPA-100; Micro-Med Inc.). The right femoral vein was catheterized for 10 mg/kg L-N^G-Nitroarginine methyl ester (LNAME) delivery. The sclera of the superior aspect of each eye was exposed, and the tip of a 1-mm diameter LDF probe connected to a blood perfusion monitor (LASERFLO BPM^2; Vasamedics, St. Paul, MN, USA) positioned between the superior and medial rectus muscles. The continuous ABP and ChBF signals were sampled at a rate of 200/second and analyzed with commercial software (LabChart 7 Pro; Colorado Springs, CO, USA). After about 30 minutes of baseline recording, LNAME in hepanized saline (10 mg/kg) was infused to assess ChBF baroregulation during high ABP for an additional 30 minutes. For analysis, we selected 10-second blocks of ABP and ChBF for every minute of stable recording and exported the value for each time block to spreadsheet software (Microsoft Corp.). To assess baroregulation, data for each rat were grouped into 5–mm Hg bins, and all ABP values within a bin were averaged to calculate the mean ABP for that bin, as were all ChBF values within that same ABP bin.

Histology – Perfusion and Tissue Harvest

After ChBF recording, rats were perfused transcardially with 150 to 200 mL of 0.9% saline and 400 to 500 mL of paraformaldehyde prepared in 0.1 M sodium phosphate buffer (pH 7.4) with 0.1 M lysine and 0.01 M sodium periodate (PLP). Eyes were removed and corneas incised. Left eyes from rats used in ChBF recordings were then immersed and stored at 4°C in EM fixative (0.5% acrolein–2% glutaraldehyde–2% paraformaldehyde in 0.1 M sodium cacodylate buffer, pH 7.2–7.4). Right eyes from these rats were infused with PLP, immersed in PLP for 2 hours at 4°C, the cornea and lens removed, and the eye stored at 4°C in 20% sucrose in 0.1 M sodium phosphate buffer (pH 7.4) with 0.02% sodium azide until cryosectioning. In the case of sham and SCGx rats that had not undergone ChBF recordings, both eyes were fixed and prepared for cryosectioning.

Immunolabeling

Sham and SCGx eyecup pairs were oriented in a mold in the same nasal–temporal orientation, surrounded by OCT compound, frozen, and sectioned across the horizontal meridian at 20 μm. The sections were processed for immunolabeling for retinal or choroidal markers, including vesicular monoamine transporter-2 (VMAT2), glial fibrillary acidic protein (GFAP), IBA1 (ionized calcium-binding adapter molecule-1), VIP, nNOS (neuronal NO synthase), and tyrosine hydroxylase (TH). Labeling was visualized either by immunofluorescence or peroxidase anti-peroxidase (PAP) methods, as described previously.[16,19] Sections prepared by immunofluorescence were viewed using a confocal laser scanning microscope (CLSM, Zeiss 710; Carl Zeiss Microscopy, Thornwood, NY, USA). For analysis of GFAP immunolabeling in Müller cells, retinal images of PAP labeling were coded for blinded quantification of GFAP upregulation with SCGx, as described previously.[25] In brief, for a 200-μm window from two randomly sampled fields from superior retina for each rat, each GFAP immunolabeled Müller cell process was scored on a 0 to 5 scale based on its penetrance into the retina from the vitread to sclerad side and the score for all processes detected summed.

TABLE. Mean ABP and ChBF

	ABP			ChBF		
	15 Min prior to LNAME	First 15 Min with LNAME	Second 15 Min with LNAME	15 Min prior to LNAME	First 15 Min with LNAME	Second 15 Min with LNAME
Sham Mean	87.7 ± 4.7 (n = 14)	137.9 ± 5.0 (n = 14)	143.2 ± 8.0 (n = 14)	16.9 ± 1.3 n = 14	15.6 ± 1.4 (n = 14)	15.1 ± 1.7 (n = 14)
SCGx Mean	94.9 ± 6.8 (n = 14)	152.0 ± 7.6 (n = 14)	160.1 ± 6.7 (n = 12)	19.4 ± 1.4 (n = 14)	19.1 ± 1.8 (n = 14)	16.1 ± 1.8 (n = 12)
SCGx as % of Sham	108.1%	110.2%	111.8%	114.5%	122.4%	106.4%

For the 15 minutes before LNAME administration, and for the two 15-minute bocks after LNAME administration. The number of eyes studied for each condition and time point is indicated in parentheses.

Retinal VMAT2 analysis was carried out using the thresholding tool of ImageJ (http://imagej.nih.gov/ij/; provided in the public domain by the National Institutes of Health, Bethesda, MD, USA), as in our prior studies.[13,19] Retinal IBA1+ microglia were manually counted blinded.

Plastic Embedding and Photoreceptor Counts

After removal from 4°C, eyes were washed in 5% sucrose/0.1 mol/l cacodylate buffer three times, cornea and lens removed, dehydrated in an ascending ethanols, and eyecups embedded in JB-4 plus or JB-4 (EMS, Hatfield, PA). We cut 5 μm–thick sections in the horizontal plane, mounted them on slides, stained them with toluidine blue, and coverslipped them with mounting medium (Permount; Thermo Fisher Scientific, Rockville, MD, USA). Images of nasal and temporal retina were captured, and photoreceptor cell bodies counted blinded in a 50-μm length of outer nuclear layer (ONL) for left eye in six sham and seven SCGx rats.

RESULTS

Choroidal Blood Flow

Baseline ABP and ChBF for each of the 15 minutes prior to LNAME were persistently elevated in SCGx eyes (by 8.1% and 14.5%, respectively), which was significant by ANOVA (ABP: $P = 0.002$; ChBF: $P = 0.000015$; Table). After LNAME infusion, ABP rose about 50 to 60 mm Hg above baseline in both groups, but was persistently greater in SCGx eyes over both each of the first and second 15 minutes after LNAME infusion (by 10.2% and 11.8%, respectively), which was significant by ANOVA (first 15 minutes: $P = 1.30 \times 10^{-7}$; second 15 minutes: $P = 8.61 \times 10^{-9}$; Fig. 1A). Over the first 5 minutes of the ABP rise after LNAME, ChBF rose briefly but minimally in sham eyes before returning to baseline, and then remained below baseline (Fig. 1A). By contrast, ChBF increased considerably more in SCGx eyes, and did not return to baseline until about 5 minutes after LNAME infusion (Fig. 1A). Even then, ChBF remained above that in sham eyes (Fig. 1B).

To assess baroregulation, we plotted ChBF as a function of ABP, with both normalized to baseline, for each of the fifteen minutes before and each of the 15 minutes commencing with LNAME administration, divided into progressive ABP bins of 5 mm Hg (Fig. 2). The slope of the relationship between ABP and ChBF over the 90% to 140% of ABP baseline range was much nearer to 1 for SCGx eyes (slope = 0.7255) than for sham (slope = 0.3828), and ABP and ChBF were highly and significantly correlated in SCGx eyes ($r = 0.951$) but were not for sham ($r = 0.483$). At ABP above 140% of baseline, ChBF decreased slightly as ABP progressively increased for both groups, but ChBF remained elevated in SCGx eyes compared to sham at any given ABP. These results show that SCGx impaired choroidal baroregulation during high ABP and led to chronically elevated ChBF as well.

ERG

For the 14 SCGx eyes examined, the scotopic ERG a- and b-wave peaks were delayed, and their amplitudes reduced compared to the 14 sham eyes. At intensities of 1 and 10 cd.s/m², the latencies for the a-wave peak were significantly slower by 5 ms for SCGx eyes (Fig. 3A), and the b-wave latency was slowed significantly at most intensities (Fig. 3C). The peak amplitude of the a-wave was higher with the brighter intensities in sham than SCGx eyes (Fig. 3B), which was most evident at 758 cd.s/m², for which the reduction in SCGx eyes was 34%. Accordingly, ANOVA for the brightest light intensities
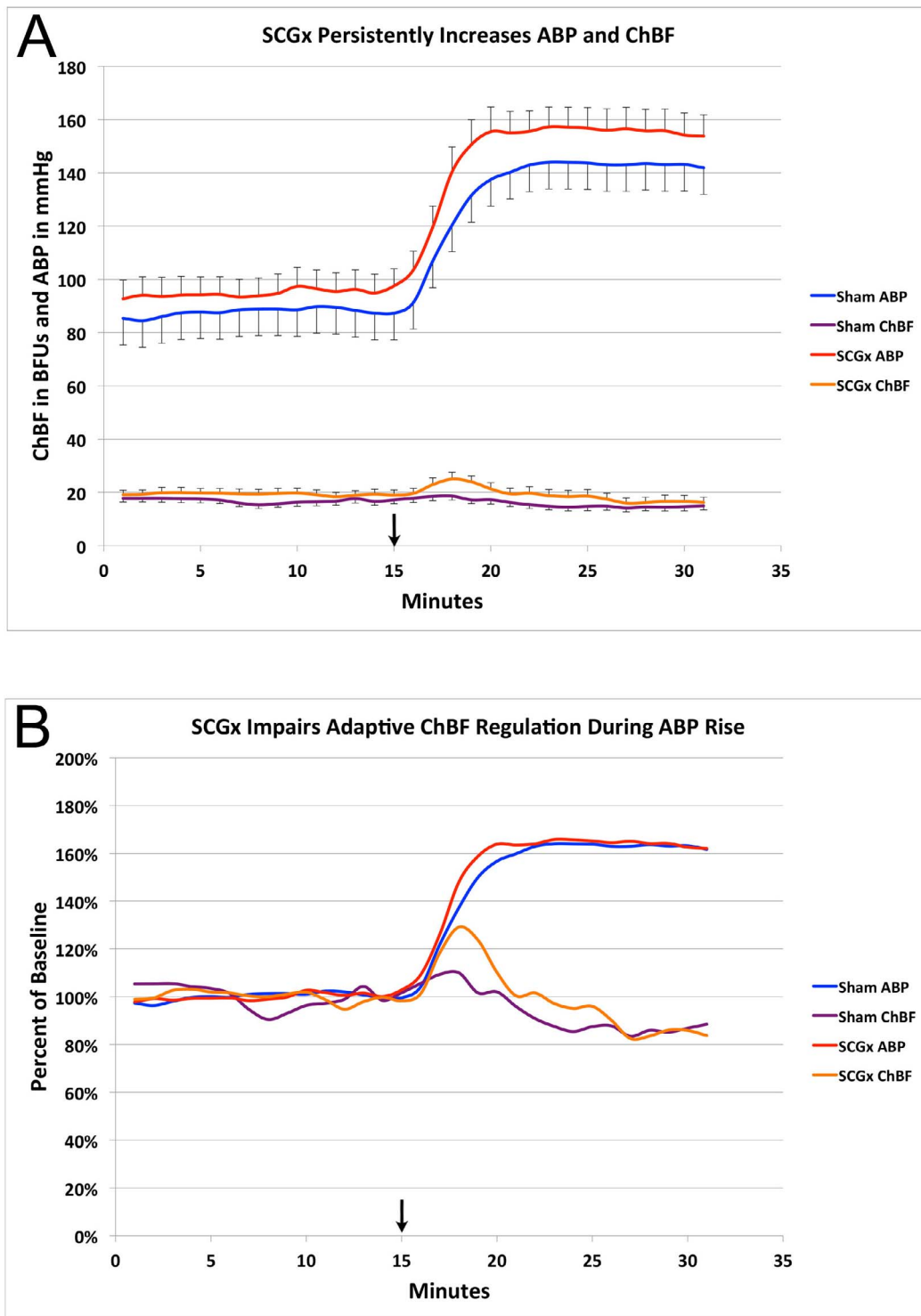
FIGURE 1. The graphs (A, B) show ChBF plotted as a function of ABP before and after administration of LNAME, with the arrows indicating the timing of LNAME administration. Graph (A) plots mean ABP in mm/Hg and ChBF per minute in arbitrary relative blood flow units (± SEM). Note that ChBF obviously rose above basal for SCGx rat eyes for the 15 minutes after LNAME administration, while ChBF in sham rats remained relatively stable. Graph (B) plots ABP and ChBF as a percent of mean pre-LNAME baseline, to better show the ChBF dynamics during the ABP rise induced by LNAME. Note that ChBF in sham eyes ($n = 14$) remained relatively flat, while that in SCGx eyes ($n = 14$) increased nearly linearly with ABP during the initial part of the ABP rise. Although ChBF subsequently declined toward baseline about 5 minutes after LNAME administration for both sham and SCGx eyes, it persistently remained elevated above sham in SCGx eyes. Thus, SCGx impaired choroidal baroregulation during high ABP, with ChBF being abnormally high.
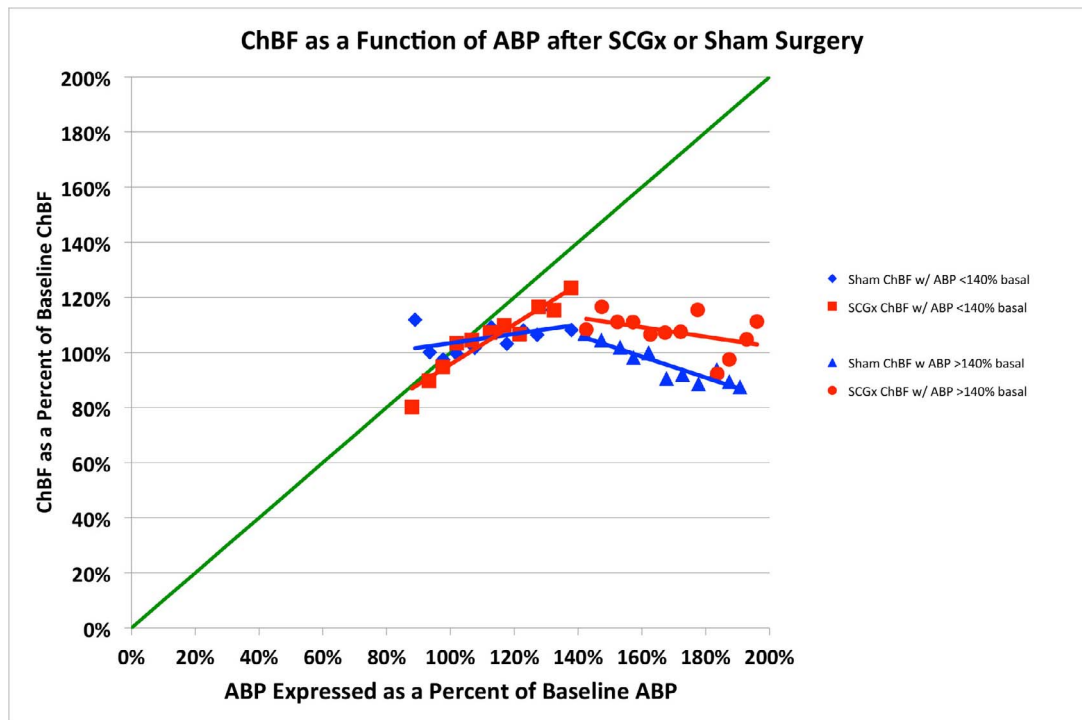
FIGURE 2. The graph shows ChBF plotted as a function of ABP for sham and SCGx rat eyes, with both expressed as a percent of basal. Mean ChBF performance is plotted per 5 mm Hg ABP bin over a range of 20 below and 100 above basal ABP. Bins are plotted for a few minutes before LNAME and then for the 10 minutes afterwards. The *green line* shows ChBF as it would be if it linearly followed ABP. Note that ChBF in sham eyes ($n = 14$) remained flat, while that in SCGx eyes ($n = 14$) increased nearly linearly with ABP until about 140 mm Hg ABP. ChBF remained relatively flat over the 140–200 mm/Hg range for both sham and SCGx. Notably, however, ChBF remained elevated above sham over the 140–200 mm/Hg range. Thus, SCGx impaired choroidal baroregulation during high ABP. ChBF rose linearly as ABP rose, and then subsequently stabilized at a high flow than was true for sham rats.

showed a significant reduction in a-wave amplitude in SCGx eyes ($P = 0.01$). ANOVA also showed a significant reduction in b-wave amplitude across light intensities in SCGx eyes ($P = 0.01$), which was noteworthy for intensities greater than 0.1 cd.s/m^2 (Fig. 3D).

Correlation analysis showed that ERG deficits were linked to ChBF regulation defects. For example, the latencies of a-wave and the b-wave across all eyes were significantly correlated with the slope of their baroregulation curves at <140 mm Hg ABP (a-wave: $r = 0.399$; b-wave: $r = 0.451$), as well as with the ABP—ChBF correlation at <140 mm Hg ABP (a-wave: $r = 0.643$; b-wave: $r = 0.543$). In other words, the a-wave and b-wave peaks were delayed (longer latency) as baroregulation failed, as reflected in an increased slope of the ABP–ChBF relationship and a higher ABP–ChBF correlation. Moreover, both the a- and b-wave peaks were significantly inversely correlated with the ABP–ChBF correlation score at ABP <140 mm Hg (a-wave: $r = 0.386$; b-wave: $r = -0.435$). Thus, as baroregulation failed (i.e., higher ABP–ChBF correlation), the a-wave peak was reduced (less negative), as was the b-wave peak (less positive).

Visual Acuity

No significant difference was seen in visual acuity between eight sham eyes and eight SCGx eyes prior to surgery ($P = 0.35843$). Two to three months after surgery, acuity in SCGx eyes was only about 50% of acuity in sham eyes (Fig. 4), a significant reduction by two-tailed t-test ($P = 0.000005$). Acuity across sham and SCGx eyes was significantly inversely correlated with the slopes of their baroregulation curves at

ABP <140 mm Hg ($r = -0.541$). Thus, as baroregulation failed (higher ABP–ChBF slope), visual acuity declined.

Structural and Neurochemical Changes in Retina and Choroid

The efficacy of the SCG removal was confirmed by the absence of VMAT2 containing sympathetic nerve fibers and terminals in SCGx choroid (Figs. 5A, 5B). Parasympathetic VIP+ fibers from PPG, however, remained abundant in choroid of sham and SCGx eyes (Figs. 5C, 5D), as did nNOS+ fibers. The VMAT2 immunolabeling allowed us to also visualize dopaminergic amacrine cells of the inner nuclear layer, which receive input from on-bipolar cells and ramify in the inner plexiform layer (IPL; Figs. 5E, 5F). The abundance of VMAT2+ terminals in IPL of SCGx eyes ($n = 7$) was significantly reduced ($P = 0.043$) to 65.6% of sham ($n = 7$; Fig. 5G). Correlation analysis revealed that the abundance of VMAT2+ terminals in IPL was significantly inversely correlated with the slope of the baroregulation curve at <140 mm Hg ABP ($r = -0.689$). Thus, as baroregulation failed (higher ABP–ChBF slope), the abundance of VMAT2 + terminals in IPL declined. A reduction in dopaminergic fibers in IPL was also seen with anti-TH immunolabeling.

GFAP in Müller cell processes was increased at 1 to 2 months after SCGx (Figs. 6A–C), with many immunolabeled processes in SCGx eyes traversing the IPL and some extending into the inner nuclear layer (INL). By contrast, in sham retinas, GFAP-immunolabeled Müller cell processes did not extend much beyond the ganglion cell layer. Using a scoring system that reflects labeled process abundance and length,[25] GFAP immunolabeling in SCGx retinas ($n = 22$) was significantly
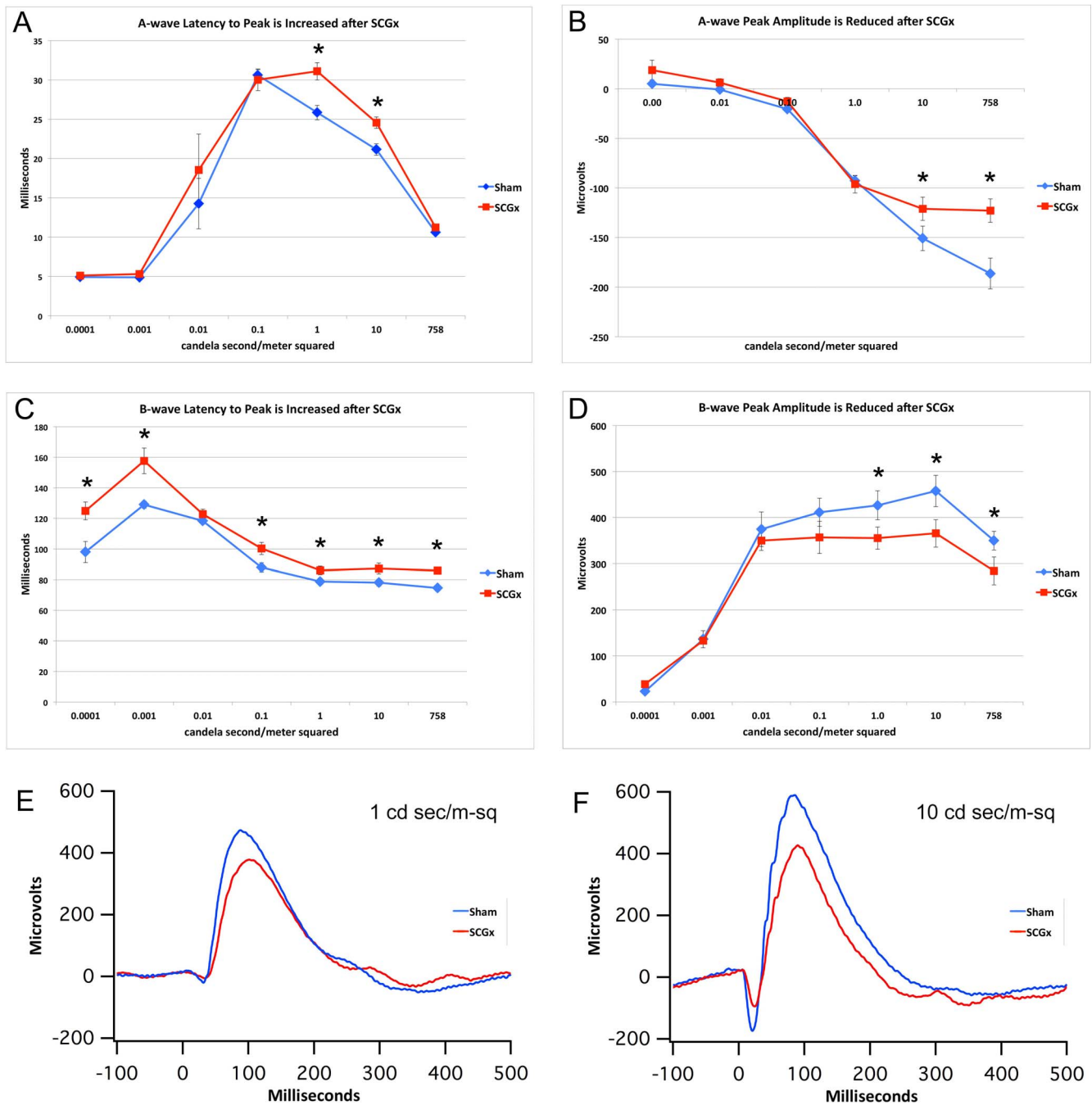
FIGURE 3. Graphs showing the mean flash-evoked scotopic a- and b-wave latencies (**A**, **C**) and peak amplitudes (**B**, **D**) for a series of light flashes 2 to 3 months after bilateral SCGx ($n = 14$), compared to sham eyes ($n = 14$). These postsurgery values for both groups are normalized to sham presurgery baseline. The b-wave peak was measured from baseline. As described in the text, the latencies were slowed and the peaks diminished for both the a-wave and b-wave for at least some light intensities in the SCGx eyes. _Asterisks_ indicate significant differences by ANOVA post hoc tests. Errors bars are SEMs. Graphs (**E**) and (**F**) show the ERG response for a sham rat (_blue_) and SCG-denervation rat (_red_) evoked by light flashes of 1 and 10 cd.s/m² (**E**, **F**, respectively).

greater (2.5-fold, $P = 0.00002$) than in sham ($n = 22$; Figs. 6D, 6E). Similarly, IBA1+ microglia in retina were significantly more abundant (3-fold, $P = 0.00274$) in SCGx retinas ($n = 5$) than in sham ($n = 5$) 1 to 3 months after surgery (Fig. 7), especially in inner retina. Too few rats that underwent ChBF measurements were used for GFAP or IBA1 immunolabeling to assess if GFAP and IBA1 elevations were correlated with baroregulatory failure. We did find, however, that the IBA1 elevation was

significantly inversely correlated with acuity—the more IBA1, the worse acuity ($r = -0.748$).

An apparent slight reduction in ONL photoreceptor cell bodies (14.7%) was seen in SCGx eyes (Fig. 8), which trended toward significance by two-tailed _t_-test ($P = 0.19692$). An adverse impact of SCGx on photoreceptors was more strongly indicated by our finding that photoreceptor abundance was significantly inversely correlated with basal ChBF ($r = -0.684$),
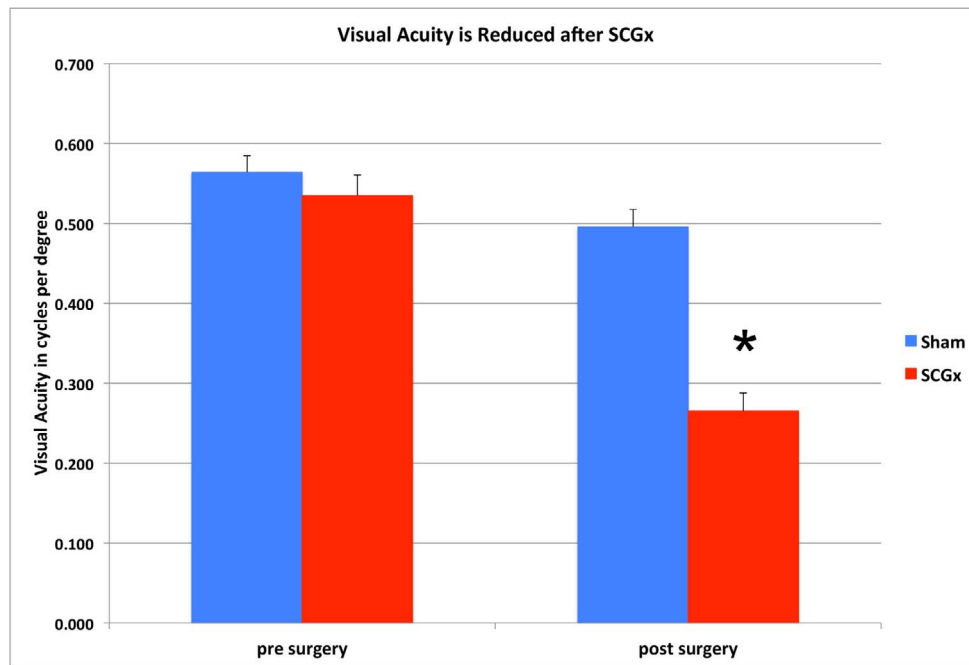
FIGURE 4. Effect of surgery on visual acuity in the eyes of sham and SCGx rats, before and 2 to 3 months after surgery, as assessed using an optokinetic system (CerebralMechanics). Acuity did not differ between sham and SCGx before surgery, but did differ significantly afterwards (*asterisk*). *Errors bars* are SEMs.

suggesting the elevated ChBF in SCGx eyes was deleterious for photoreceptor survival. Among visual parameters, photoreceptor abundance was significantly inversely correlated with a-wave latency ($r = -0.634$) and trended toward being inversely correlated with a-wave peak ($r = -0.457$). Thus, loss of photoreceptors was linked to a-wave slowing (increased latency) and perhaps a reduced (more positive) a-wave peak.

DISCUSSION

Our studies indicate that sympathetic denervation of choroid impairs ChBF baroregulation during upward ABP fluctuations and increases basal ChBF, causing choroidal overperfusion. These defects have a pathological effect on retina by 1 to 3 months post SCGx. These findings and their implications are discussed in more detail below.

Sympathetic Control of Choroidal Blood Flow

Sympathetic noradrenergic nerve fibers from SCG innervate choroid,[1,2,26-32] and mediate decreases in ChBF[33-39] via alpha-adrenergic receptors,[6,38-44] as well as by NPY action.[45,46] Although earlier studies in rabbits using labeled microspheres had reported that sympathetic denervation does not substantially affect basal choroidal tone at normal BP,[6,7,9,17,47] more recent studies have shown increased choroidal vessel luminal diameters 6 weeks after cranial sympathetic transection in rats,[48] and choroidal expansion by 6 weeks after superior cervical ganglion removal in mice.[49] Consistent with the vasodilatory effect of removal of sympathetic vasoconstrictory tone implied by the latter studies, we observed by LDF that basal ChBF was slightly but persistently elevated in SCGx compared to sham eyes (by 14.5%) at 2 to 3 months after surgery. Steinle et al.[48] as well also reported increased basal ChBF after cranial sympathetic transection in rats.

Bill[6,7,50] has suggested that sympathetic innervation of choroid becomes activated with elevated BP. Studies in humans have shown, in fact, that the choroid vasoconstricts after exercise-induced increases in systemic BP and thereby compensates for the increased perfusion pressure.[11,12] Our results indicate that central baroreceptor-responsive circuitry acting via sympathetic input to choroid contributes to choroidal baroregulation during high systemic BP, as well as to basal tone. The baroregulatory impairment we observed with SCGx appears to involve failure of two components that maintain ChBF near basal levels during elevated ABP, one that acts as ABP rises rapidly and one that acts during a sustained elevation. Our results show that some non-sympathetic mechanism must also contribute to the latter, since even in the absence of SCG innervation ChBF returns toward baseline after the initial ABP rise, although ChBF remains elevated. It is uncertain if the non-sympathetic vasoconstriction is mediated by diminished parasympathetic tone or by non-neural autoregulatory mechanisms, such as endothelial vasoconstrictor release[51] or myogenic mechanisms.[52]

Choroidal Sympathetic Control and Retinal Health

In the absence of sympathetic contributions to basal choroidal tone and baroregulation during high BP, the resulting sustained ChBF increase leads to overperfusion and breakdown of the blood-retinal barrier.[7-10,53] Consistent with an adverse effect of overperfusion on retina, a significant increase in Müller cell GFAP and 30% reduction in photoreceptor cell bodies have been reported in rats 6 weeks after cranial sympathetic transection[54] and apoptosis among photoreceptor cell bodies and a diminished ERG a-wave peak was reported 10 weeks after SCGx in mice.[49] In the present study, we confirmed GFAP upregulation and photoreceptor loss after SCGx, and additionally observed loss of dopaminergic amacrine cell processes and increases in retinal microglia. We also found that scotopic flash-evoked ERG a-wave and b-wave latencies were slowed, and
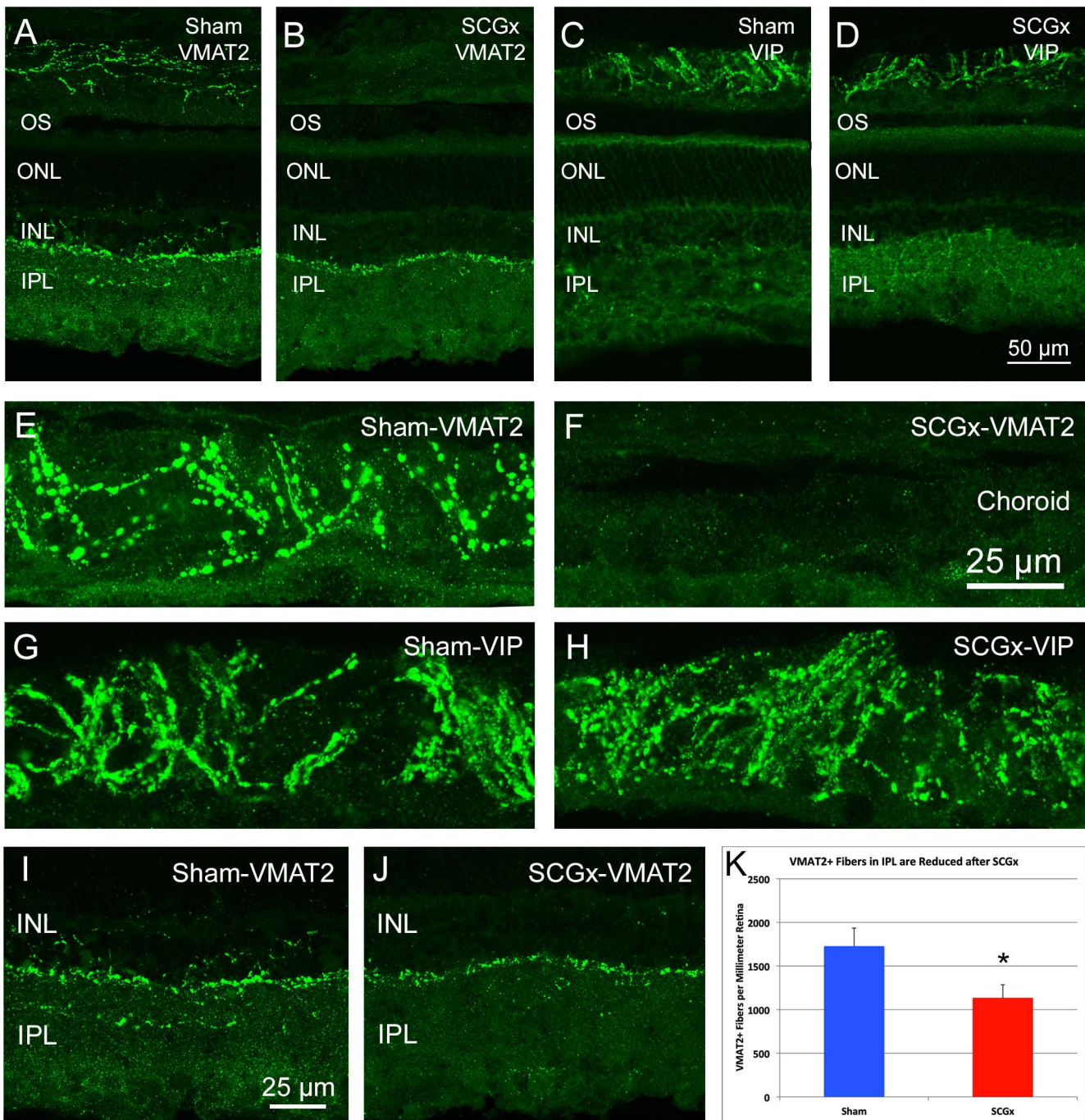
FIGURE 5. Effects of superior cervical ganglion removal on sympathetic and parasympathetic innervation of choroid (**A–H**) as shown in low power view of the entire retina and choroid (**A–D**) and high power view of the choroid alone (**E–H**), and on VMAT2+ fibers in retina as shown in high power view (**I–K**). Abundant sympathetic fibers, revealed by VMAT2 immunolabeling, are present in the choroid of the sham eyes (**A, E**), whereas no sympathetic fibers were detected by VMAT2 immunostaining in the choroid of SCGx rats (**B, F**), which confirmed that the bilateral SCG removal had been successful. By contrast, parasympathetic innervation of choroid was intact following SCGx, as revealed by VIP immunolabeling of sham (**C, G**) and SCGx (**D, H**) eyes. Similar results were seen for parasympathetic fibers immunolabeled for nNOS (not shown). The abundance of the VMAT2+ terminals of dopaminergic amacrine cells in the IPL of SCGx eyes (**B, I**) was reduced to about half of that in sham (**A, J**). The graph in (**K**) shows quantitative analysis of the significant reduction (*asterisk*) in VMAT2+ terminals in the IPL of SCGx retinas, as determined using analysis of CLSM images of VMAT2 immunolabeling using ImageJ. The scale in (**D**) applies to images (**A–D**), that in (**F**) applies to (**E–H**), and that in (**I**) also applies to (**J**).

ERG amplitudes and visual acuity reduced. The GFAP upregulation is broadly indicative of retinal pathology after SCGx, and the increase in microglia suggests retinal inflammation following choroidal overperfusion. Importantly, we found that the failure of baroregulation was significantly correlated with the slowing of the latencies and reductions in the peaks of a- and b-waves, and to the decline in visual acuity. Photoreceptors, however, seemed more affected by the increase in basal ChBF in SCGx eyes. Since dopamine receptor antagonists reduce the ERG b-wave,[55] the reduction in retinal VMAT2 may
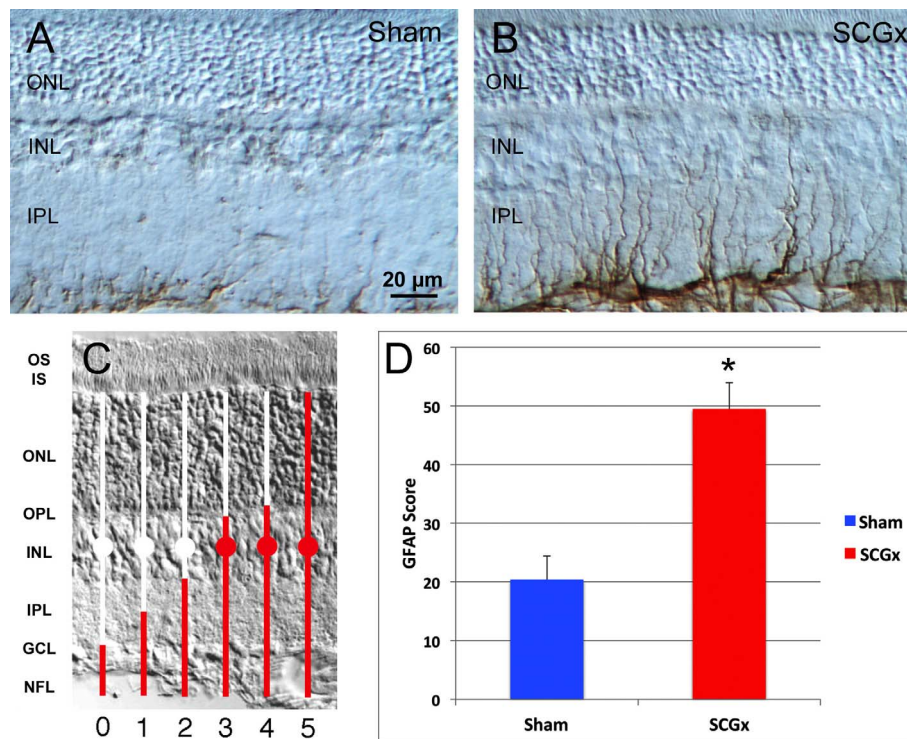
FIGURE 6. Effects of SCGx on GFAP immunolabeling of Müller cell processes in sham (**A**) versus SCGx (**B**) retina. The GFAP+ Müller cell processes in SCGx eyes traversed the IPL and some extended into the inner nuclear layer (INL) (**B**). By contrast, in control retinas, GFAP labeling of Müller cell processes did not extend much beyond the ganglion cell layer (GCL) (**A**). Using a scoring system for the GFAP immunolabeling (**C**), GFAP labeling in SCGx retinas at a mean survival of 45 days was significantly elevated (*asterisk*) above that in sham retinas by ×2.5 (**D**). The GFAP immunolabeling score for each retina reflects both the abundance and sclerad penetrance of the GFAP immunolabeled Müller cell processes per 200 μm retinal length. The *scale bar* in (**A**) also applies to (**B**). IS, inner segments; NFL, nerve fiber layer; ON, outer nuclear layer; OPL, outer plexiform layer; OS, outer segments.

contribute to b-wave reduction in SCGx eyes. Note that pupil constriction caused by SCGx is unlikely to contribute to the retinal dysfunction or pathology we observed, since constriction would reduce light stress on the retina and aid acuity performance. Moreover, in the case of ERGs, pupils were dilated pharmacologically, so any SCGx impact on pupil was obviated.

The means by which choroidal overperfusion injures retina is uncertain, but it is likely heightened oxygen tension resulting from choroidal overperfusion increases reactive oxygen species (ROS) and oxidative stress, and thereby damages outer retinal proteins, carbohydrates and lipids,[56–59] hindering function and causing apoptosis.[58,60] The increases in retinal microglia following SCGx are consistent with the possibility that the injury provokes an inflammatory response,[61,62] leading microglia to produce proinflammatory and cytotoxic mediators that hinder repair and contribute to neuronal dysfunction and cell death.[63]

Implications of Current Findings

Many diseases or conditions affecting retina have impaired ChBF as concomitants, including AMD,[64–75] chronic hypertension,[76,77] insulin-dependent diabetes,[78] glaucoma,[79–82] ischemic outer retinal disease,[83] myopic retinopathy,[84] central serous chorioretinopathy,[85] and aging.[13,21,66,86–88] Disturbances in neurogenic maintenance of basal tone or adaptive ChBF responses could be contributing factors to retinal declines seen in these diseases or conditions, although loss and narrowing of choroidal vessels may also contribute as well.[27,76,89–92] Much of the attention on disease-related ChBF

impairments has focused on diminished ChBF. Nonetheless, sympathetic control of choroid is also impaired with aging,[93,94] and defects in choroidal baroregulation during high systemic BP occur in aging[95,96] and wet AMD.[68] Told et al.[14] found that a CFH risk factor for AMD (i.e., CC complement factor H haplotype) was associated with impaired baroregulation of ChBF during high BP in young risk-gene carriers. The similar impairment in ChBF baroregulation seen later in symptomatic AMD[68] suggests that impairment in hypertensive ChBF baroregulation may begin early in life and persist. Our studies show that chronic impairment of sympathetic regulation of ChBF leads to outer retinal injury, and thus could contribute to AMD pathogenesis.

The study of the Schmetterer group, however, does not rule out the possibility of defects in hypotensive parasympathetic baroregulation as well. Given the evidence for reduced ChBF in symptomatic AMD,[64–75] it would be of value to know how early in the lifespan defects in sympathetic and/or parasympathetic regulation of ChBF occur, and whether they are driven by genetic AMD risk factors, as well as by nongenetic risk factors such as smoking.[97] Both impaired parasympathetic and sympathetic ChBF control might be especially insidious, since it would yield alternating underperfusion and overperfusion that could cause ongoing ischemia-reperfusion injury, which is known to prominently drive ROS production.[57] The outer retinal injury associated with impaired ChBF regulation may lead to waste accumulation in and along Bruch's membrane as seen in normal aging.[89,98–100] In those with a pro-AMD genetic predisposition or risk factors, the waste may trigger the
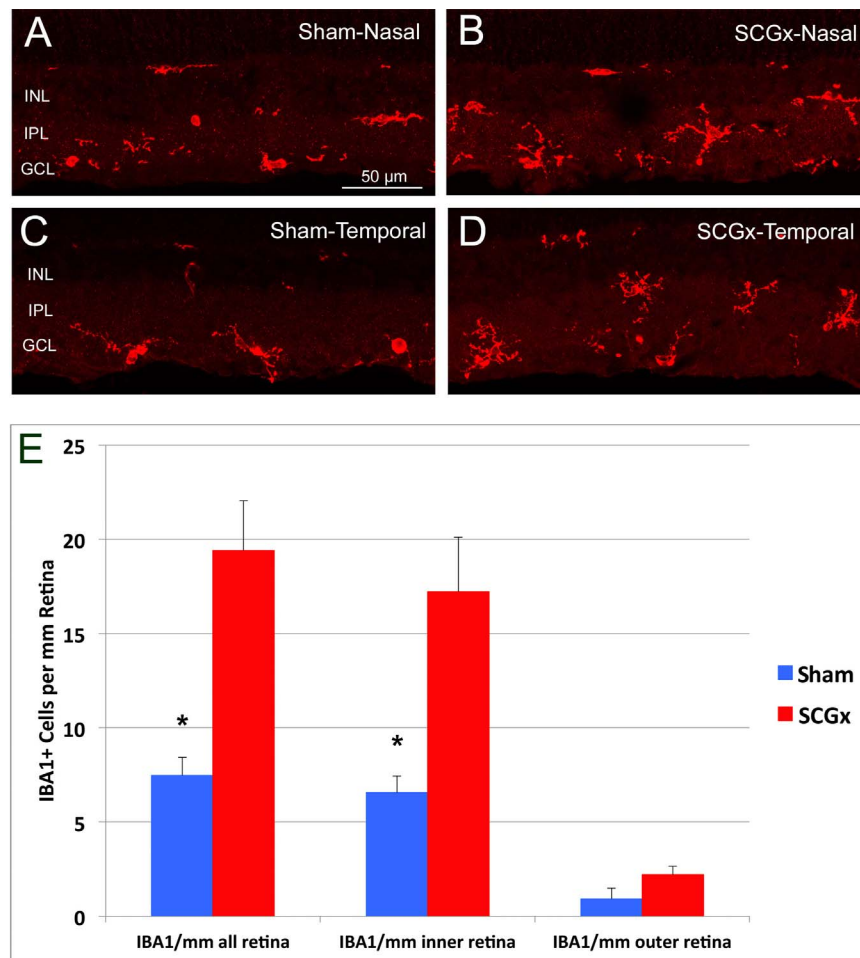
FIGURE 7. Microglia in the IPL as detected by IBA1 immunolabeling (**A–D**) were three times more abundant in retina 2 to 3 months after SCGx than in sham retina (**E**), especially in the inner retina. IBA1-immunolabeled microglia were counted blindly in images captured by CLSM. These results suggest a pathological inflammatory process in the inner retina following SCGx. The scale in (**A**) also applies to (**B–D**).
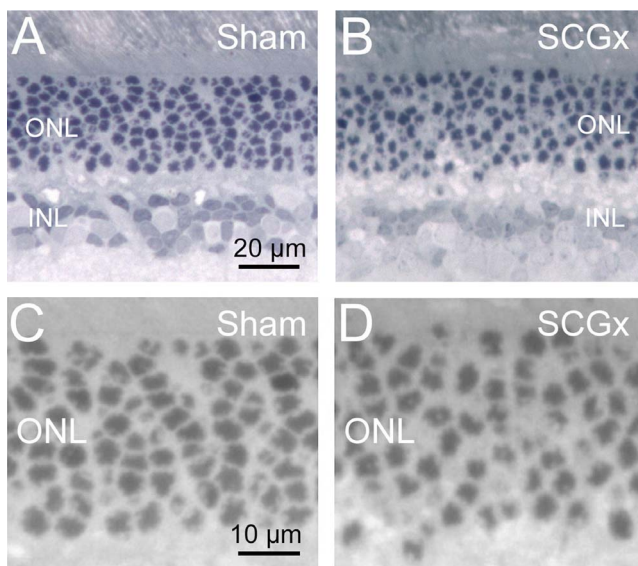

FIGURE 8. Images of sections through sham (**A**, **C**) and SCGx (**B**, **D**) retina showing a slight apparent reduction in photoreceptor cell body abundance in the outer nuclear layer (ONL) in SCGx retina. The scale in (**A**) also applies to (**B**), and that in (**C**) also applies to (**D**).

complement factor-mediated inflammatory outer retinal injury of AMD.[71,101,102]

Acknowledgments

Disclosure: **C. Li**, None; **M.E.C. Fitzgerald**, None; **N. Del Mar**, None; **C. Haughey**, None; **A. Reiner**, None

References

1. Stone RA, Kuwayama Y, Laties AM. Regulatory peptides in the eye. *Experientia*. 1987;43:791–800.

2. Li H, Grimes P. Adrenergic innervation of the choroid and iris in diabetic rats. *Current Eye Res*. 1993;12:89–94.

3. Reiner A, Fitzgerald MEC, Li C. Neural control of ocular blood flow. In: *Ocular Blood Flow*. Schmetter L, J Kiel J, ed. Heidelberg, Germany: Springer-Verlag; 2012:243–309.

4. Reiner A, Fitzgerald MEC, Del Mar N, Li C. Neural control of choroidal blood flow. *Prog Retinal Eye Res*. 2018;64:96–130.

5. Reiner A, Li C, Del Mar N, Fitzgerald MEC. Choroidal blood flow compensation in rats for arterial blood pressure decreases is neuronal nitric oxide-dependent but compensation for arterial blood pressure increases is not. *Exp Eye Res*. 2010;90:734–741.

6. Bill A. The circulation in the eye. In: Renkin EM, Michel CC, eds. *Handbook of Physiology: The Cardiovascular System IV: Microcirculation, Part 2*. Baltimore, MD: Waverly Press; 1984:1001–1035.

7. Bill A, Linder M, Linder J. The protective role of ocular sympathetic vasomotor nerves in acute arterial hypertension. *Bibl Anat*. 1977;16:30–35.

8. Bill A. Effect of acute hemorrhaging in rabbits on blood circulation in the eye and various other tissues. The role of the sympathetic nerves [in German]. *Klin Monbl Augenheilkd*. 1984;184:305–307.

9. Bill A, Nilsson SF. Control of ocular blood flow. *J Cardiovasc Pharmacol*. 1985;7:S96–S102.

10. Ernest JT. The effect of systolic hypertension on rhesus monkey eyes after ocular sympathectomy. *Am J Ophthalmol*. 1977;84:341–344.

11. Riva CE, Titze P, Hero M, Movaffaghy A, Petrig BL. Choroidal blood flow during isometric exercises. *Invest Ophthalmol Vis Sci*. 1997;38:2338–2343.

12. Lovasik JV, Kergoat H, Riva CE, Petrig BL, Geiser M. Choroidal blood flow during exercise-induced changes in the ocular perfusion pressure. *Invest Ophthalmol Vis Sci*. 2003;44:2126–2132.

13. Jablonski MM, Iannaccone A, Reynolds, et al. Age-related decline in VIP-positive parasympathetic nerve fibers in the human submacular choroid. *Invest Ophthalmol Vis Sci*. 2007;48:479–485.

14. Told R, Palkovits S, Haslacher H, et al. Alterations of choroidal blood flow regulation in young healthy subjects with complement factor H polymorphism. *PLoS One*. 2013; 8:e60424.

15. Savastano LE, Castro AE, Fitt MR, Rath MF, Romeo HE, Muñoz EM. A standardized surgical technique for rat superior cervical ganglionectomy. *J Neurosci Methods*. 2010;192: 22–33.

16. Li C, Fitzgerald MEC, Cuthbertson S, et al. A pseudorabies virus transneuronal tracing study characterizing the central neurons responsible for parasympathetic regulation of choroidal blood flow in rat eye. *Front Syst Neurosci*. 2015; 9:65.

17. Chou PI, Lu DW, Chen JT. Effect of sympathetic denervation on rabbit choroidal blood flow. *Ophthalmologica*. 2002;216: 60–64.

18. Prusky GT, Alam NM, Beekman S, Douglas RM. Rapid quantification of adult and developing mouse spatial vision using a virtual optomotor system. *Invest Ophthalmol Vis Sci*. 2004;45:4611–4616.

19. Guley NH, Rogers JT, Del Mar NA, et al. A novel closed-head model of mild traumatic brain injury using focal primary overpressure blast to the cranium in mice. *J Neurotrauma*. 2016;33:403–422.

20. Fitzgerald ME, Gamlin PD, Zagvazdin Y, Reiner A. Central neural circuits for the light-mediated reflexive control of choroidal blood flow in the pigeon eye: a laser Doppler study. *Vis Neurosci*. 1996;13:655–669.

21. Fitzgerald ME, Tolley E, Frase S, et al. Functional and morphological assessment of age-related changes in the choroid and outer retina in pigeons. *Vis Neurosci*. 2001;18: 299–317.

22. Zagvazdin Y, Fitzgerald MEC, Reiner A. Role of muscarinic cholinergic transmission in Edinger-Westphal nucleus-induced choroidal vasodilation in pigeon. *Exp Eye Res*. 2000; 70:315–327.

23. Li C, Fitzgerald MEC, Del Mar N, Reiner A. Stimulation of the nucleus of solitary-tract produces choroidal vasodilation in rats. *Front Neuroanat*. 2016;10:94.

24. Li C, Fitzgerald MEC, Del Mar N, Reiner A. Disinhibition of neurons of the nucleus of solitary tract that project to the superior salivatory nucleus causes choroidal vasodilation: Implications for mechanisms underlying choroidal baroregulation. *Neurosci Letters*. 2016;633:106–111.

25. Kimble TD, Fitzgerald ME, Reiner A. Sustained upregulation of glial fibrillary acidic protein in Müller cells in pigeon retina following disruption of the parasympathetic control of choroidal blood flow. *Exp Eye Res*. 2006;83:1017–1030.

26. Fitzgerald ME, Caldwell RB, Reiner A. Vasoactive intestinal polypeptide-containing nerve fibers are increased in abundance in the choroid of dystrophic RCS rats. *Curr Eye Res*. 1992;11:501–515.

27. Frank RN. Studies in diabetic retinopathy. In: Tso MOM, ed. *Retinal Disease: Biomedical Foundations & Clinical Management*. Philadelphia, PA: Lippincott Co; 1988:165–180.

28. Malmfors T. The adrenergic innervation of the eye as demonstrated by fluorescence microscopy. *Acta Physiol Scand*. 1965;65:259–267.

29. Laties AM, Jacobowitz D. A comparative study of the autonomic innervation of the eye in monkey, cat and rabbit. *Anat Rec*. 1966;162:501–504.

30. Ehinger B. Adrenergic nerves to the eye and to related structures in man and the cynomolgus monkey. *Invest Ophthalmol*. 1966;5:42–52.

31. Klooster J, Beckers HJ, Ten Tusscher MP, Vrensen GFJM, van der Want JL, Lamers WPMA. Sympathetic innervation of the rat choroid: an autoradiographic tracing and immunohistochemical study. *Ophthalmic Res*. 1996;28:36–43.

32. Smith PG, Fan Q. Sympathetic nerve trajectories to rat orbital targets: role of connective tissue pathways. *J Comp Neurol*. 1996;365:69–78.

33. Bill A. Autonomic nervous control of uveal blood flow. *Acta Physiol Scand*. 1962;56:70–81.

34. Alm A, Bill A. The effect of stimulation of the cervical sympathetic chain on retinal oxygen tension and on uveal, retinal and cerebral blood flow in cats. *Acta Physiol Scand*. 1973;88:84–94.

35. Alm A. The effect of sympathetic stimulation on blood flow through the uvea, retina and optic nerve in monkeys (*Macacca irus*). *Exp Eye Res*. 1977;25:19–24.

36. Alm A. Ocular circulation. In: Hart WM, ed. *Adler's Physiology of the Eye: Clinical Application*. St Louis: Mosby; 1992:198–227.

37. Riva CE, Cranstoun SD, Mann RM, Barnes GE. Local choroidal blood flow in the cat by laser Doppler flowmetry. *Invest Ophthalmol Vis Sci*. 1994;35:608–618.

38. Abe S, Karita K, Izumi H, Tamai M. Increased and decreased choroidal blood flow elicited by cervical sympathetic nerve stimulation in the cat. *Jpn J Physiol*. 1995;45:347–353.

39. Steinle JJ, Smith PG. Presynaptic muscarinic facilitation of parasympathetic neurotransmission after sympathectomy in the rat choroid. *J Pharmacol Exp Ther*. 2000;294627–632.

40. Gherezghiher T, Okubo H, Koss MC. Choroidal and ciliary body blood flow analysis: application of laser Doppler flowmetry in experimental animals. *Exp Eye Res*. 1991;53: 151–156.

41. Koss MC. Adrenoceptor mechanisms in epinephrine-induced anterior choroidal vasoconstriction in cats. *Exp Eye Res*. 1994;59:715–722.

42. Koss MC, Gherezghiher T. Adrenoceptor subtypes involved in neurally evoked sympathetic vasoconstriction in the anterior choroid of cats. *Exp Eye Res*. 1993;57:441–447.

43. Kawarai M, Koss MC. Sympathetic vasoconstriction in the rat anterior choroid is mediated by alpha1-adrenoceptors. *Eur J Pharmacol*. 1998;363:35–40.

44. Kiel JW, Lovell MO. Adrenergic modulation of choroidal blood flow in the rabbit. *Invest Ophthalmol Vis Sci*. 1996; 37:673–679.

45. Nilsson SF. Neuropeptide Y (NPY): a vasoconstrictor in the eye, brain and other tissues in the rabbit. *Acta Physiol Scand*. 1991;141:455–467.

46. Bill A. The 1990 Endre Balazs lecture. Effects of some neuropeptides on the uvea. *Exp Eye Res*. 1991;53:3–11.

47. Chou P, Lu DW, Chen JT. Bilateral superior cervical ganglionectomy increases choroidal blood flow in the rabbit. *Ophthalmologica*. 2000;214:421–425.

48. Steinle JJ, Pierce JD, Clancy RL, Smith PG. Increased ocular blood vessel numbers and sizes following chronic sympathectomy in rat. *Exp Eye Res*. 2002;74:761–768.

49. Dieguez HH, Romeo HE, González Fleitas MF, et al. Superior cervical gangliectomy induces non-exudative age-related macular degeneration in mice. *Dis Model Mech*. 2018;11:2.

50. Bill A. Some aspects of the ocular circulation. Friedenwald lecture. *Invest Ophthalmol Vis Sci*. 1985;26:410–424.

51. Fuchsjäger-Mayrl G, Luksch A, Malec M, Polska E, Wolzt M, Schmetterer L. Role of endothelin-1 in choroidal blood flow regulation during isometric exercise in healthy humans. *Inves. Ophthalmol Vis Sci*. 2003;44:728–733.

52. Kiel JW. Choroidal myogenic autoregulation and intraocular pressure. *Exp Eye Res*. 1994;58:529–543.

53. Bill A, Linder J. Sympathetic control of cerebral blood flow in acute arterial hypertension. *Acta Physiol Scand*. 1976;96: 114–121.

54. Steinle JJ, Lindsay NL, Lashbrook BL. Cervical sympathectomy causes photoreceptor-specific cell death in the rat retina. *Auton Neurosci*. 2005;120:46–51.

55. Huppé-Gourgues F, Coudé G, Lachapelle P, Casanova C. Effects of the intravitreal administration of dopaminergic ligands on the b-wave amplitude of the rabbit electroretinogram. *Vision Res*. 2005;45:137–145.

56. Bill A, Sperber GO. Control of retinal and choroidal blood flow. *Eye (Lond)*. 1990;4:319–325.

57. Beatty S, Koh H, Phil M, Henson D, Boulton M. The role of oxidative stress in the pathogenesis of age-related macular degeneration. *Surv Ophthalmol*. 2000;45:115–134.

58. Gore A, Muralidhar M, Espey MG, Degenhardt K, Mantell LL. Hyperoxia sensing: from molecular mechanisms to significance in disease. *J Immunotoxicol*. 2010;7:239–254.

59. Vlachantoni D, Bramall AN, Murphy MP, et al. Evidence of severe mitochondrial oxidative stress and a protective effect of low oxygen in mouse models of inherited photoreceptor degeneration. *Human Mol Gen*. 2011;20:322–335.

60. Terraneo L, Samaja M. Comparative response of brain to chronic hypoxia and hyperoxia. *Int J Mol Sci*. 2017;18.

61. Buchanan MM, Hutchinson M, Watkins LR, Yin H. Toll-like receptor-4 in CNS pathologies. *J Neurochem*. 2010;114:13–17.

62. Tornatore L, Thotakura AK, Bennett J, Moretti M, Franzoso G. The nuclear factor kappa B signaling pathway: integrating metabolism with inflammation. *Trends Cell Biol*. 2012;22: 557–566

63. Loane DJ, Kumar A. Microglia in the TBI brain: the good, the bad, and the dysregulated. *Exp Neurol*. 2016;275:316–327.

64. Friedman E, Krupsky S, Lane AM, et al. Ocular blood flow velocity in age-related macular degeneration. *Ophthalmology*. 1995;102:640–646.

65. Grunwald JE, Hariprasad SM, DuPont J, et al. Foveolar choroidal blood flow in age-related macular degeneration. *Invest Ophthalmol Vis Sci*. 1998;39:385–390.

66. Grunwald JE, Metelitsina TI, DuPont J, et al. Reduced foveolar choroidal blood flow in eyes with increasing AMD severity. *Invest Ophthalmol Vis Sci*. 2005;46:1033–1038.

67. Ciulla TA, Harris A, Martin BJ. Ocular perfusion and age-related macular degeneration. *Acta Ophthalmol Scand*. 2001;79:108–115.

68. Pournaras CJ, Logean E, Riva CE, et al. Regulation of subfoveal choroidal blood flow in age-related macular degeneration. *Invest Ophthalmol Vis Sci*. 2006;47:1581–1586.

69. Metelitsina TI, Grunwald JE, DuPont JC, Ying GS, Brucker AJ, Dunaief JL. Foveolar choroidal circulation and choroidal neovascularization in age-related macular degeneration. *Invest Ophthalmol Vis Sci*. 2008;49:358–363.

70. Pemp B, Schmetterer L. Ocular blood flow in diabetes and age-related macular degeneration. *Can J Ophthalmol*. 2008; 43:295–301.

71. Feigl B. Age-related maculopathy—linking aetiology and pathophysiological changes to the ischaemia hypothesis. *Prog Retinal Eye Res*. 2009;28:63–86.

72. Bhutto IA, Baba T, Merges C, McLeod DS, Lutty GA. Low nitric oxide synthases (NOS) in eyes with age-related macular degeneration (AMD). *Exp Eye Res*. 2010;90:155–167.

73. Boltz A, Luksch A, Wimpissinger B, et al. Choroidal blood flow and progression of age-related macular degeneration in the fellow eye in patients with unilateral choroidal neovascularization. *Invest Ophthalmol Vis Sci*. 2010;51: 4220–4225.

74. Xu W, Grunwald JE, Metelitsina TI, et al. Association of risk factors for choroidal neovascularization in age-related macular degeneration with decreased foveolar choroidal circulation. *Am J Ophthamol*. 2010;150:40–47.

75. Berenberg TL, Metelitsina TI, Madow B, et al. The association between drusen extent and foveolar choroidal blood flow in age-related macular degeneration. *Retina*. 2012;32:25–31.

76. Tso MOM, Jampol LM. Hypertensive retinopathy, choroidopathy & optic neuropathy of hypertensive ocular disease. In: Laragh JH, Brenner BM, eds. *Hypertension: Pathophysiology, Diagnosis & Management*. New York, NY: Raven Press; 1990:433–465.

77. Haefliger IO, Flammer J, Beny JL, Lüscher TF. Endothelium-dependent vasoactive modulation in the ophthalmic circulation. *Prog Retin Eye Res*. 2001;20,209–225.

78. Langham ME, Grebe R, Hopkins S, Marcus S, Sebag M. Choroidal blood flow in diabetic retinopathy. *Exp Eye Res*. 1991;52:167–173.

79. James CB, Smith SE. Pulsatile ocular blood flow in patients with low tension glaucoma. *Br J Ophthalmol*. 1991;75:466–470.

80. Kubota T, Jonas JB, Naumann GO. Decreased choroidal thickness in eyes with secondary angle closure glaucoma. An aetiological factor for deep retinal changes in glaucoma? *Br J Ophthalmol*. 1993;77:430–432.

81. Grunwald JE, Piltz J, Hariprasad SM, DuPont J. Optic nerve and choroidal circulation in glaucoma. *Invest Ophthalmol Vis Sci*. 1998;39:2329–2336.

82. Su WW, Cheng ST, Hsu TS, Ho WJ. Abnormal flow-mediated vasodilation in normal-tension glaucoma using a noninvasive

determination for peripheral endothelial dysfunction. *Invest Ophthalmol Vis Sci*. 2006;47:3390–3394.

83. Gaudric A, Coscas G, Bird AC. Choroidal ischemia. *Am J Ophthalmol*. 1982;94:489–498.

84. Blacharski P. Pathological progressive myopia. In: Newsome DA, ed. *Retinal Dystrophies and Degenerations*. New York, NY: Raven Press; 1988:257–269.

85. Tittl M, Maar N, Polska E, Weigert G, Stur M, Schmetterer L. Choroidal hemodynamic changes during isometric exercise in patients with inactive central serous chorioretinopathy. *Invest Ophthalmol Vis Sci*. 2005;46:4717–4721.

86. Yoneya S, Amano H, Mori K, Ohki R, Deguchi T. Indocyanine green angiography of the choroid in young and aged eyes. *Invest Ophthalmol Vis Sci*. 1995;36:S187.

87. Emeterio Nateras OS, JM, Harrison Muir ER, et al. Choroidal blood flow decreases with age, an MRI study. *Curr Eye Res*. 2014;39:1059–1067.

88. Whitmore SS, Sohn EH, Chirco KR, et al. Complement activation and choriocapillaris loss in early AMD: implications for pathophysiology and therapy. *Prog Retinal Eye Res*. 2015;45:1–29.

89. Tso MO. Photic injury to the retina and pathogenesis of age-related macular degeneration. In: *Retinal Diseases: Biomedical Foundations & Clinical Management*. Philadelphia, PA: Lippincott Co; 1988:187–214.

90. Ramrattan RS, van der Schaft TL, Mooy CM, de Bruijn WC, Mulder PG, de Jong PT. Morphometric analysis of Bruch's membrane, the choriocapillaris, and the choroid in aging. *Invest Ophthalmol Vis Sci*. 1994;35:2857–2864.

91. Spraul CW, Lang GE, Grossniklaus HE. Morphometric analysis of the choroid, Bruch's membrane, and retinal pigment epithelium in eyes with age-related macular degeneration. *Invest Ophthalmol Vis Sci*. 1996;37:2724–2735.

92. Grunwald JE, Hariprasad SM, DuPont J. Effect of aging on foveolar choroidal circulation. *Arch Ophthalmol*. 1998;116:150–154.

93. Smith CP, Sharma S, Steinle JJ. Age-related changes in sympathetic neurotransmission in rat retina and choroid. *Exp Eye Res*. 2007;84:71–81.

94. Nuzzi R, Finazzo C, Grignolo FM. Changes in adrenergic innervation of the choroid during aging. *J Fr Ophthalmol*. 2010;19:89–96.

95. Reiner A, Li C, Del Mar N, Zagvazdin Y, Fitzgerald MEC. Age-related impairment in choroidal blood flow compensation for arterial blood pressure fluctuation in pigeons. *Invest Ophthalmol Vis Sci*. 2011;52:7238–7247.

96. Dallinger S, Findl O, Strenn K, Eichler HG, Wolzt M, Schmetterer L. Age dependence of choroidal blood flow. *J Am Geriatr Soc*. 1998;46:484–487.

97. Wimpissinger B, Resch H, Berisha F, Weigert G, Polak K, Schmetterer L. Effects of isometric exercise on subfoveal choroidal blood flow in smokers and nonsmokers. *Invest Ophthalmol Vis Sci*. 2003;44:4859–4863.

98. Potts AM. An hypothesis on macular disease. *Trans Am Acad Ophthalmol Otolaryngol*. 1966;70:1058–1062.

99. Herron WL, Riegel BW, Myers OE, Rubin ML. Retinal dystrophy in the rat–a pigment epithelial disease. *Invest. Ophthalmol*. 1969;8:595–604.

100. LaVail MM. Analysis of neurological mutants with inherited retinal degeneration. Friedenwald lecture. *Invest Ophthalmol Vis Sci*. 1981;21:638–657.

101. Winkler BS, Boulton ME, Gottsch JD, Sternberg P. Oxidative damage and age-related macular degeneration. *Mol Vis*. 1999;5:32.

102. Hageman GS, Gaehrs K, Johnson LV, Anderson D. Age-Related Macular Degeneration (AMD). 2018. Available at: https://webvision.med.utah.edu/book/part-xii-cell-biology-of-retinal-degenerations/age-related-macular-degeneration-amd/. Accessed September 28, 2018.